International Journal Of
Industrial Electronics Control and Optimization
Print ISSN: 3517-2645
Online ISSN: 3568-2645
Homepage: https://ieco.usb.ac.ir/

Enhanced Speed Loop Control Strategy for Yokeless Axial Flux-Switching Permanent Magnet Motors

Javad Rahmani-Fard | Saeed Hasanzadeh
Department of Electrical and Computer Engineering, Qom University of Technology, Qom, Iran
Corresponding Author Email: rahmanifard@qut.ac.ir

Article Info

Article type:
Research Article

Article history:
Received: 28-May-2024
Received in revised form: 10-December-2024
Accepted:28-December-2024
Published online: 23-Sep-2025

Keywords:
Sliding Mode Control,
Flux-Switching motor,
Fault-tolerant,
EVs.

ABSTRACT

This paper presents an Enhanced Model-Free Sliding Mode Control (EMFSMC) method tailored for the speed loop of a 12-slot/19-pole yokeless and segmented armature axial flux-switching permanent magnet (12S/19P YASA-AFFSSPM) motor, focusing on robustness against parameter perturbations. Traditional control techniques, such as Proportional-Integral (PI) control and Model-Free Sliding Mode Control (MFSMC), have shown limitations in handling the motor's nonlinear behavior and susceptibility to disturbances. The proposed EMFSMC algorithm optimizes speed loop performance by establishing a hyperlocal model of the YASA-AFFSSPM motor, which accounts for parameter variations. An improved double-power combinatorial reaching law is developed to enhance convergence rates during the sliding surface approach phase, while an Extended Sliding Mode Disturbance Observer (ESMDO) provides real-time monitoring of unknown disturbances affecting speed control. Simulation results demonstrate that the EMFSMC significantly accelerates the speed response time to approximately 0.015 seconds with minimal overshoot, compared to 0.04 seconds and a 12.5% overshoot with the MFSMC. Additionally, under sudden load conditions, the EMFSMC controller exhibits a speed drop of only 4 rpm, recovering to stability in about 0.01 seconds, while the MFSMC controller experiences a 9 rpm drop with a recovery time of 0.03 seconds. These findings confirm that the EMFSMC enhances the speed response rate and robustness of the speed loop, outperforming traditional control methodologies across various operating conditions.

NOMENCLATURE

u_d, u_q	d-q axis voltages	s	Sliding variable
R_{so}	Nominal value of the stator phase winding resistance	L_{do}, L_{qo}	Nominal values of the stator winding d-q axis inductances
i_d, i_q	d-q axis current components	α, β	Exponents in the reaching law
k_1, k_2,k_3	Positive constants used in reaching laws	ε_1, ε_2	Exponential parameters in the reaching law
ω_e	Rotor electrical angular velocity	x_1, x_2	State variables of speed error and its integral
ψ_{ro}	Permanent magnet flux linkage	s_1	Sliding surface for speed error
J	Moment of inertia	s_2	Sliding surface for speed estimation error
ΔR_s	Perturbation of resistance	ζ, δ	Parameters in the extended hyper-local model
ΔL_d, ΔL_q	Perturbations of the stator inductance parameters	F	Unknown part of the system
$\Delta\psi_r$	Variation of the magnetic flux linkage of the permanent magnet	$\hat{F}$	Real-time estimation of the unknown part of the system
T_e	Output electromagnetic torque	$\hat{\omega}$	Real-time speed estimation
n_p	Number of rotor poles	u_c	Control input of the speed loop feedback controller
ΔT_e	Torque disturbance due to parameter perturbation	$\omega_{e}*$	Given speed of the motor
Δu_d, Δu_q	Uncertain quantities caused by parameter changes in the d-axis and q-axis	l	Observer gain in the extended sliding mode disturbance observer
$R(t)$	Rate of change of the unknown quantity	s	Sliding variable
η_1, η_2	Positive constants in the observer control law	k_1, k_2,k_3	Positive constants used in reaching laws

Copyright © J. Rahmani-Fard (s).
Publisher: University of Sistan and Baluchestan

I. Introduction

Permanent Magnet Synchronous Motors (PMSMs) play a crucial role in various industries, serving as a cornerstone in applications that demand high precision and efficiency, such as robotics, aerospace, automotive, and renewable energy systems. In recent times, a specific type of PMSM known as the Flux Switching Permanent Magnet (FSPM) motor has emerged as a promising alternative, offering advancements in power density and control flexibility [1-2]. The 12Slots/19 poles yokeless and segmented armature flux-switching sandwiched permanent magnet (12S/19P YASA-AFFSSPM) machines represent an innovative category of flux machines with a unique topology. This design provides several benefits, including increased torque density, minimized cogging torque, and electrical as well as magnetic isolation between phases [3, 4]. Consequently, the 12S/19P YASA-AFFSSPM configuration shows significant potential as an in-wheel direct drive motor for Electric Vehicles (EVs). Since the system equations of FSPM motors closely resemble those of PMSMs, control strategies developed for PMSMs can be effectively adapted for FSPM motors.

While traditional Proportional-Integral (PI) control is simple and easy to implement, it lacks robustness against external disturbances and changes in system parameters due to the nonlinear and strongly coupled nature of Permanent Magnet Synchronous Motors (PMSMs). To address this limitation, advanced control methods such as model predictive control [5], model-free control [6], neural network control [7], and sliding mode control [8] have been proposed. Model-free control is notable for its insensitivity to both internal and external disturbances and its robustness in scenarios where dynamic effects on the system are poorly modeled. Sliding mode control also offers advantages in insensitivity to parameter variations and strong robustness. Thus, combining sliding mode control with model-free control effectively reduces the reliance on accurate motor system models and mitigates the impacts of system parameter changes and external disturbances. However, integrating sliding mode control and model-free control can introduce chattering, which is a common issue with sliding mode methods. Therefore, enhancing system response speed while reducing chattering has become a primary focus in model-free sliding mode control research. Approaches like the one suggested in [9] are often used to lessen chattering. In robotic systems, Reference [10] developed a model-free control scheme that combines adaptive dynamic sliding mode control with a voltage control strategy, addressing uncertainties in practical applications by estimating lumped uncertainty, thus improving tracking performance and ensuring system stability, as validated through simulation results. Building on this, References [11] and [12] introduced double power-law and multi-power-law approach laws to expedite convergence rates and minimize chattering through the incorporation of power-law terms. Subsequently, Reference [13] proposed double power-law combination approach laws derived from the double power-law approach laws, enhancing system performance across different states. Recent advancements in control strategies, particularly sliding mode control (SMC), have shown promise in managing chaotic systems with uncertainties. Reference [14] illustrates that SMC can stabilize time-varying chaotic systems by defining a sliding surface that mitigates the effects of disturbances, ensuring fixed-time stability. Reference [15] effectively reduced chattering by using an extended state observer for improved estimation accuracy compared to traditional observers [16]. However, challenges such as managing multiple parameters and intricate tuning arose. To address these issues, Reference [17] developed an extended sliding mode disturbance observer, enhancing system robustness. Additionally, Reference [18] introduced an adaptive fuzzy fractional-order fast terminal sliding mode control approach, employing a novel fractional-order sliding surface and fuzzy system to eliminate chattering and ensuring finite-time stability via Lyapunov's theorem.

To tackle parameter perturbations affecting the robustness of control systems for the 12-slot/19-pole yokeless and segmented armature axial flux-switching sandwiched permanent magnet (12S/19P YASA-AFFSSPM) motor, this study presents the Enhanced Model-Free Sliding Mode Control (EMFSMC) algorithm. This algorithm features a novel double-power combination sliding mode reaching law to enhance convergence rates during the sliding mode approach while reducing chattering. The integration of the Extended Sliding Mode Disturbance Observer (ESMDO) allows for real-time monitoring and estimation of unknown disturbances affecting speed control, improving overall accuracy and stability.

Simulation and experimental results indicate that EMFSMC outperforms MFSMC in speed response time, stability, and robustness under various operating conditions, leading to significant reductions in speed drop and recovery time during sudden load changes. These advancements enhance the performance of the YASA-AFFSSPM motor, making it a promising candidate for applications in electric vehicles and other precision-demanding industries. Comprehensive validations demonstrate the effectiveness of the proposed control algorithms in significantly improving the performance of the 12S/19P YASA-AFFSSPM motor.

II. Configuration

In [3], a novel motor structure without yoke and armature segmentation is proposed to maximize slot space and coil winding capacity, thereby enhancing the slot fill factor and torque density. The YASA-AFFSSPM motor, depicted in Fig. 1, features a stator with 12 modular units, each containing 3 "I"-shaped stator teeth, 2 "I"-shaped permanent

magnets, and 1 winding coil. This yokeless stator design optimizes coil winding space, resulting in increased average torque output. The motor also uses two rotors positioned 180 degrees apart electrically, which effectively eliminates high-order harmonics of back-EMF and reduces cogging torque.

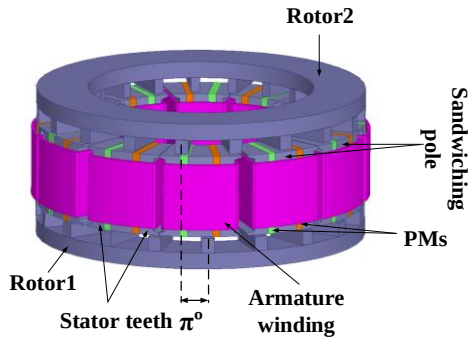

Fig. 1. Machine topology.

$$\begin{cases} u_d = R_{\mathrm{so}} i_d + L_{do}\frac{\mathrm{d}i_d}{\mathrm{d}t} - \omega_{\mathrm{e}} L_{q0} i_q + \Delta u_d \\ u_q = R_{\mathrm{so}} i_q + L_{q0}\frac{\mathrm{d}i_q}{\mathrm{d}t} + \omega_{\mathrm{e}} L_{d0} i_d + \omega_{\mathrm{e}}\psi_{\mathrm{ro}} + \Delta u_q \end{cases} \quad (1)$$

Here, u_d and u_q are the d-q axis voltages; R_{so} is the nominal value of the stator phase winding resistance; i_d and i_q are the d-q axis current components; L_{do} and L_{qo} are the nominal values of the stator winding *d-q* axis inductances; ω_e is the rotor electrical angular velocity; ψ_{ro} is the nominal value of the PM flux linkage; Δu_d and Δu_q are the uncertain quantities caused by parameter changes in the *d*-axis and *q*-axis of the motor, expressed as :

$$\begin{cases} \Delta u_d = \Delta R_s i_d + \Delta L_d\frac{\mathrm{d}i_d}{\mathrm{d}t} - \omega_{\mathrm{e}}\Delta L_q i_q \\ \Delta u_q = \Delta R_s i_q + \Delta L_q\frac{\mathrm{d}i_q}{\mathrm{d}t} - \omega_{\mathrm{e}}\Delta L_d i_d + \omega_{\mathrm{e}}\Delta\psi_{\mathrm{r}} \end{cases} \quad (2)$$

Here, where, ΔR_s is the perturbation of resistance, ΔL_d and ΔL_q are the perturbations of the stator inductance parameters; $\Delta\psi_r$ is the variation of the magnetic flux linkage of the permanent magnet. The electromagnetic torque equation is given by:

$$\begin{aligned} T_e &= \frac{3}{2} n_p[\psi_{ro} + (L_d - L_q) i_d] i_q + \Delta T_e \\ &= \tfrac{3}{2} n_p \psi_{ext} i_q + \Delta T_e \end{aligned} \quad (3)$$

where $\psi_{\mathrm{ext}} = \psi_{\mathrm{ro}} + (L_d - L_q) i_d$ is effective magnetic flux linkage, T_e represents the output electromagnetic torque, n_p is the rotor poles number and ΔT_e represents the torque disturbance due to parameter perturbation, expressed as:

$$\Delta T_{\mathrm{e}} = \tfrac{3}{2} n_{\mathrm{p}}[\Delta\psi_{\mathrm{r}} + (\Delta L_d - \Delta L_q) i_d] i_q \quad (4)$$

The mechanical motion equation in the d-q coordinate system is given by:

$$T_e = T_{\mathrm{L}} + \frac{J}{n_{\mathrm{p}}}\frac{\mathrm{d}\omega_e}{\mathrm{d}t} + B\omega_{\mathrm{m}} \quad (5)$$

here, T_L represents the load torque, J is the moment of inertia, B is the torque damping coefficient, and $B\omega_m$ is the damping torque. By combining Equations (3) and (5), the speed state equation of YASA-AFFSSPM under parameter perturbation can be obtained as

$$\frac{\mathrm{d}\omega_{\mathrm{e}}}{\mathrm{d}t} = \tfrac{3}{2}\frac{n_{\mathrm{p}}^2}{J}\psi_{\mathrm{ext}} i_q - \frac{B}{J}\omega_{\mathrm{e}} + \frac{n_{\mathrm{p}}}{J}(\Delta T_{\mathrm{e}} - T_{\mathrm{L}}) \quad (6)$$

III. Controller Design

A. Improved reaching Law Design

Reference [13] indicates that the double-power reaching law outperforms other reaching laws such as the constant-speed, exponential. The double-power reaching law is expressed as:

$$\dot{s} = -k_1|s|^{\alpha}\mathrm{sgn}(s) - k_2|s|^{\beta}\mathrm{sgn}(s) \quad (7)$$

The double-power combined reaching law exhibits superior performance compared to both the double-power reaching law and the fast-power reaching law. Therefore, this paper proposes a new reaching law based on the double-power combined reaching law, represented as:

$$\dot{s} = \begin{cases} \begin{pmatrix} -k_1|s|^{\alpha}\,\mathrm{sgn}(s) \\ -k_2|s|^{\beta}\,\mathrm{sgn}(s) - \varepsilon_1|x_1|^{\lambda_1}s \end{pmatrix}, & |s| > 1 \\ \begin{pmatrix} -k_1|s|^{\alpha}\mathrm{sgn}(s) \\ -k_3 s - \varepsilon_2|x_1|^{\lambda_2}s \end{pmatrix}, & |s| \leqslant 1 \end{cases} \quad (8)$$

In Eq.s (7) and (8): k_1, k_2, k_3, ε_1, ε_2 are all greater than 0; $0<\alpha$; $\lambda_2<1$; $1<\beta$, λ_1 and *sgn*(*s*) denotes the sign function. The new reaching law introduces exponential terms $\varepsilon_1|x_1|^{\lambda_1}s$ and $\varepsilon_2|x_1|^{\lambda_2}s$ to improve the convergence rate. Moreover, by introducing the state variables x_1 the exponential parameter can be adaptively changed. Through proper setting of all parameters, it can effectively suppress vibration generation.

B. Analysis of Convergence Rate of Enhanced reaching Law

Assuming the initial state $\boldsymbol{s}$ is $s(0)$, and $s(0)>1$, the convergence process of the system can be divided into two stages.

$s(0)\rightarrow s(T1)=1$, where $T1$ is the required time. For Eq. (8), since $0<\alpha$, $\lambda 2<1$, and $1<\beta$, $\lambda 1$, the $k_1|s|^{\alpha}\mathrm{sgn}(s) \ll k_2|s|^{\beta}\mathrm{sgn}(s) + \varepsilon_1|x_1|^{\lambda_1}s$ convergence rate in this stage is mainly affected by $-k_2|s|^{\beta}\,\mathrm{sgn}(s) - \varepsilon_1|x_1|^{\lambda_1}s$. The reaching law (8) can be written

$$\dot{s} = -k_2|s|^{\beta}\mathrm{sgn}(s) - \varepsilon_1|x_1|^{\lambda_1}s \quad (9)$$

Solving equations with multiple power terms is somewhat challenging. They can be considered as multiple equations to solve and compare separately. Thus, Equation (9) can be divided into $\dot{s} = -k_2|s|^{\beta}\mathrm{sgn}(s)$ and $\dot{s} = -\varepsilon|x_1|^{\lambda_1}s$, respectively. By separately considering the convergence rate under the influence of $-k_2|s|^{\beta}\mathrm{sgn}(s)$ and $-\varepsilon|x_1|^{\lambda_1}s$, the required convergence time for this stage of the new convergent rate must be less than either of the two solutions.

Solving $\dot{s} = -k_2|s|^{\beta}\mathrm{sgn}(s)$, and rearranging the original equation, we get

$$\frac{\dot{s}}{s^{\beta}} = -k_2 \quad (10)$$

Let t_0 be the time taken by $s(0)\rightarrow s(t_0)=1$ under the influence of $\dot{s} = -k_2|s|^{\beta}\mathrm{sgn}(s)$ only. Integrating Eq. (10) from $t=0$ to $t=t_0$ to get the convergence time t_0 as

$$t_0 = \frac{1-s(0)^{1-\beta}}{k_2(\beta-1)} \tag{11}$$

Solving can be obtained for $\dot{s} = -\varepsilon|x_1|^{\lambda_1}s$. Arrange the original equation to get:

$$\frac{\dot{s}}{|x_1|^{\lambda_1}s} = -\varepsilon_1 \tag{12}$$

Let t_1 be the time taken by $s(0)\rightarrow s(t_1)=1$ under the influence of only $\dot{s} = -\varepsilon|x_1|^{\lambda_1}s$. Integrating Eq.(12) from $t=0$ to $t=t_1$, the convergence time t_1 can be obtained:

$$t_1 = -\frac{1}{\varepsilon_1}\int_0^t \frac{1}{|x_1|^{\lambda_1}}\,\mathrm{d}(\ln\, s) \tag{13}$$

Therefore, for the new reaching law, the time T_1 required from $s(0)$ to $s(T_1)$ is

$$T_1 \leqslant \min(t_0, t_1) \tag{14}$$

2) $s(T_1)\rightarrow s(t)=0$, let the required time be T_2. For equation (8), since $0<\alpha$, $\lambda 2<1$, $1<\beta$, $\lambda 1$ and $k_3 s \ll k_1|s|^{\alpha}\mathrm{sgn}\,(s) + \varepsilon_2|x_1|^{\lambda_2}s$, the convergent rate at this stage is mainly affected by $k_1|s|^{\alpha}\mathrm{sgn}\,(s) + \varepsilon_2|x_1|^{\lambda_2}s$ and the convergent law (8) can be written as

$$\dot{s} = -k_1|s|^{\alpha}\mathrm{sgn}\,(s) - \varepsilon_2|x_1|^{\lambda_2}s \tag{15}$$

Similarly, Equation (15) can be divided into $\dot{s} = -k_1|s|^{\alpha}\mathrm{sgn}\,(s)$ and $\dot{s} = -\varepsilon_2|x_1|^{\lambda_2}s$. By separately considering the convergence rate under the influence of $k_1|s|^{\alpha}\mathrm{sgn}\,(s)$ and $\varepsilon_2|x_1|^{\lambda_2}s$, the required convergence time in this stage must be less than either of the two solutions.

Solving $\dot{s} = -k_1|s|^{\alpha}\mathrm{sgn}\,(s)$ and rearranging the original equation, we get

$$\frac{\dot{s}}{s^{\alpha}} = -k_1 \tag{16}$$

Let $t2$ be the time required for $s(T1)\rightarrow s(t2')=0$ under the sole action of $\dot{s} = -k_1|s|^{\alpha}\mathrm{sgn}\,(s)$. Thus, integrating both sides of equation (16) from $t=T_1$ to $t=t_2'$, we can obtain the approximate time t_2.

$$t_2 = \frac{1}{k_1(1-\alpha)} \tag{17}$$

The given equation is $\dot{s} = -\varepsilon_2|x_1|^{\lambda_2}s$. Upon rearranging:

$$\frac{\dot{s}}{|x_1|^{k_2}s} = -\varepsilon_2 \tag{18}$$

Similarly, let t_3 be the time required for $s(T_1)\rightarrow s(t'_3)=0$ under the sole action of $s = -\varepsilon_2|x_1|^{\lambda_2}s$. Thus, integrating both sides of equation (18) from $t=T_1$ to $t=t'_3$, we can obtain the approximate time t_3.

$$t_3 = -\frac{1}{\varepsilon_2}\int_{T_1}^{t_3'} \frac{1}{|x_1|^{\lambda_2}}\,\mathrm{d}(\ln s) \tag{19}$$

Therefore, for the new modeled approximation law, the time T_2 required for $s(T_1)$ to reach $s(t)=0$ is obtained as:

$$T_2 \leqslant \min(t_2, t_3) \tag{20}$$

To sum up, it can be seen that the convergence time of the new reaching law is approximately $T=T_1+T_2 \leq t_0+t_2$, and the convergence time of the double power combination reaching law is approximately $T_3=t_0+t_2$. Additionally, it is known that the convergence time of the double power-law convergence law is T_4+T_3. Thus, we have $T \leq T_3 < T_4$. Therefore, the new reaching law exhibits superior convergence speed compared to both the double power reaching law and the double-power combined reaching law.

C. Analysis on the Existence and Reachability of reaching Law

The theorem states that when the initial state of the system $s(0)$ is not on the sliding surface, then the system state can asymptotically converge to the sliding surface under the action of the sliding mode convergence law (8).

Proof: Let the Lyapunov function be $V=s^2/2$. According to equation (8), we can obtain the relationship can be obtained as:

$$\dot{V} = s\dot{s} = \begin{cases} s\begin{bmatrix} -k_1|s|^{\alpha}\mathrm{sgn}\,(s) \\ -\varepsilon|x_1|^{\lambda_1}s \\ -k_2|s|^{\beta}\,sgn(s)) \end{bmatrix} < 0, |s| > 1 \\ s\begin{bmatrix} -k_1|s|^{\alpha}\,\mathrm{sgn}(s)) \\ -k_3 s \\ -\varepsilon|x_1|^{\lambda_2}s \end{bmatrix} \leqslant 0, \quad |s| \leqslant 1 \end{cases} \tag{21}$$

From equation (21), we can see that $\dot{V} = s\dot{s} = 0$ if and only if $s=0$. According to the conditions of existence and reachability of reaching law, if the designed reaching law satisfies the Lyapunov stability condition, namely, if the first-order derivative of the Lyapunov function V is negative ($\dot{V} < 0$), then the reaching law is both existent and reachable. Therefore, the reaching law (8) can lead the system state to asymptotically converge to the sliding surface.

D. Design of improved model-free sliding mode controller for speed loop

Based on the hyperlocal model theory [20], a hyperlocal model of the speed loop is established based on the input and output of the YASA-AFFSSPM motor speed loop.

$$\dot{\omega}_e = F + \alpha i_q \tag{22}$$

where, α represents the to-be-designed q-axis stator current parameter, and F represents the known part of the system as well as the uncertain parameters.

Based on the hyper-local model [20], the model-free controller for the speed loop can be designed as follows.

$$i_q = \frac{-F+\dot{\omega}_e^*+u_c}{\alpha} \tag{23}$$

Here, ω_e^* is the given speed of the motor; u_c is the control input of the speed loop feedback controller. By combining Equation (22) and Equation (23), we can obtain:

$$(\dot{\omega}_e^* - \dot{\omega}_e) + u_c = 0 \tag{24}$$

Designing the speed loop feedback controller as a sliding mode controller allows for the integration of model-free control with sliding mode control methods. Using the YASA-AFFSSPM speed error as a state variable:

$$\begin{cases} x_1 = \omega_e^* - \omega_e \\ x_2 = \int x_1\,\mathrm{d}t \end{cases} \tag{25}$$

By combining Equation (24) and Equation (25), and then differentiating Equation (25), we obtain:

$$\begin{cases} \dot{x}_1 = -u_c \\ \dot{x}_2 = \omega_e^* - \omega_e \end{cases} \tag{26}$$

Select the sliding surface as

$$s_1 = x_1 + cx_2 \tag{27}$$

where c is a parameter to be designed, and $c>0$. Differentiating Equation (27) and substituting Equation (26), we get:

$$\dot{s}_1 = cx_1 - u_c \tag{28}$$

To improve the convergence rate during the sliding mode approach phase and reduce chattering during the sliding phase, we select an improved double power combination reaching law for designing the controller. Therefore, by combining Equation (8), (26), and (28), we obtain:

$$u_c = \begin{cases} \begin{pmatrix} c(\omega_e^* - \omega_e) + k_1|s_1|^{\alpha} sgn(s_1) \\ +k_2|s_1|^{\beta} \operatorname{sgn}(s_1) + \varepsilon|x_1|^{\lambda_1} s_1 \end{pmatrix}, |s_1| > 1 \\ \begin{pmatrix} c(\omega_e^* - \omega_e) + k_1|s_1|^{\alpha} sgn(s_1) \\ +k_3 s_1 + \varepsilon|x_1|^{\lambda_2} s_1 \end{pmatrix}, |s_1| \leqslant 1 \end{cases} \quad (29)$$

In order to ensure stability of the designed controller, the sliding mode reachability condition needs to be satisfied:

$$\dot{V}_1 = s_1 \dot{s}_1 \leqslant 0 \quad (30)$$

We select the Lyapunov function $V_1=s_1^2/2$. Since we choose the improved reaching law as the sliding mode convergence rate, substituting equations (28) and (29) into the function (30), we obtain:

$$\dot{V}_1 = s_1 \dot{s}_1 = \begin{cases} s_1 \cdot \begin{bmatrix} -k_1|s_1|^{\alpha} \operatorname{sgn}(s_1) \\ -\varepsilon|x_1|^{\lambda_1} s_1 \\ -k_2|s_1|^{\beta} \operatorname{sgn}(s_1) \end{bmatrix}, |s_1| > 1 \\ s_1 \cdot \begin{bmatrix} -k_1|s_1|^{\alpha} \operatorname{sgn}(s_1) \\ -k_3 s_1 - \varepsilon|x_1|^{\lambda_2} s_1 \end{bmatrix}, |s_1| \leq 1 \end{cases} \quad (31)$$

From equation (31), we can see that the controller satisfies the sliding mode reachability condition. By combining equations (23) and (29), we obtain the designed YASA-AFFSSPM motor vector control system's speed loop improved model-free sliding mode control law:

$$i_q = \begin{cases} \frac{1}{\alpha} \begin{pmatrix} -F + \dot{\omega}_e^* + c(\omega_e^* - \omega_e) \\ +k_1|s_1|^{\alpha} \operatorname{sgn}(s_1) \\ +\varepsilon|x_1|^{\lambda_1} s_1 \\ +k_2|s_1|^{\beta} \operatorname{sgn}(s_1) \end{pmatrix} |s_1| > 1 \\ \frac{1}{\alpha} \begin{pmatrix} -F + \dot{\omega}_e^* + c(\omega_e^* - \omega_e) \\ +k_1|s_1|^{\alpha} \operatorname{sgn}(s_1) \\ +k_3 s_1 + \varepsilon|x_1|^{\lambda_2} s_1 \end{pmatrix} |s_1| \leq 1 \end{cases} \quad (32)$$

E. ESMDO Design

From the control law equation (32), we can see that there exist unknown parts F in the system. Therefore, we design an extended sliding mode disturbance observer to observe and compensate for the unknown part *F*. The extended hyper-local model for YASA-AFFSSPM motor is given by:

$$\begin{cases} \frac{d\omega_c}{dt} = \zeta i_q - \delta \omega_e + F \\ \frac{dF}{dt} = R(t) \end{cases} \quad (33)$$

In equation (33), R(t) represents the rate of change of the unknown quantity *F*, and ζ and δ are parameters to be designed. For equation (33), the system is designed with the following extended sliding mode disturbance observer as:

$$\begin{cases} \frac{d\hat{\omega}_e}{dt} = \zeta i_q - \delta \omega_e + \hat{F} + u_{\text{smo}} \\ \frac{d\hat{F}}{dt} = l u_{\text{smo}} \end{cases} \quad (34)$$

In the equation $\hat{\omega}$ represents the real-time speed estimation, $\hat{F}$ represents the real-time estimation of the unknown part of the system, u_{smo} is the sliding mode function to be designed, *l* is the observer u_{smo} gain.

By combining equations (33) and (34), the observation error is given by:

$$\begin{cases} \dot{x} = \delta x + \tilde{F} + u_{smo} \\ \frac{d\tilde{F}}{dt} = l u_{smo} - R(t) \end{cases} \quad (35)$$

The error terms are as follows: speed estimation error: $\dot{x} = \hat{\omega}_e - \omega_e$, system disturbance observation error: $\tilde{F} = \hat{F} - F$. We choose the speed error as the sliding surface s_2 as:

$$s_2 = \dot{x} = \hat{\omega}_e - \omega_e \quad (36)$$

To ensure performance during the sliding mode approach phase, we choose exponential convergence law for the reaching law:

$$\dot{s}_2 = -\eta_1 \operatorname{sgn}(x) - \eta_2 x \quad (37)$$

where η_1 and η_2 are positive constants. Then, the sliding mode observer control law u_{smo} is:

$$u_{smo} = -\delta x - \tilde{F} - \eta_1 \operatorname{sgn}(x) - \eta_2 x \quad (38)$$

Theorem 2: If we choose equation (36) as the sliding surface, and $\eta_1 \geq \|\tilde{F}\|$, then the observer in equation (34) is asymptotically stable.

Proof: Let the Lyapunov function be $V_2 = s_2^2/2$.

$$\begin{aligned} &\dot{V}_2 = \dot{s}_2 s_2 = x\left(\delta x + \tilde{F} + u_{\text{smo}}\right) = \\ &x\left(\tilde{F} - \eta_1 \operatorname{sgn}(x) - \eta_2 x\right) = \\ &x\tilde{F} - \eta_1 x \operatorname{sgn}(x) - \eta_2 x^2 \leqslant \|x\|\left(\|\tilde{F}\| - \eta_1\right) \end{aligned} \quad (39)$$

Therefore, as long as $\eta_1 \leq \|\tilde{F}\|$, $\dot{V} \leq 0$ is guaranteed.

$$\hat{F} = l \int \left(-\delta x - \eta_1 \operatorname{sgn}(x) - \eta_2 x\right) dt \quad (40)$$

Substituting the observed value $\hat{F}$ obtained from equation (40) into equation (32), we obtain the model-free sliding mode control law for the speed loop as:

$$i_q = \begin{cases} \frac{1}{\alpha} \begin{pmatrix} -\hat{F} + \dot{\omega}_e^* + c(\omega_e^* - \omega_e) \\ +k_1|s_1|^{\alpha} \operatorname{sgn}(s_1) \\ +\varepsilon|x_1|^{\lambda_1} s_1 \\ +k_2|s_1|^{\beta} \operatorname{sgn}(s_1) \end{pmatrix} |s_1| > 1 \\ \frac{1}{\alpha} \begin{pmatrix} -F + \dot{\omega}_e^* + c(\omega_e^* - \omega_e) \\ +k_1|s_1|^{\alpha} \operatorname{sgn}(s_1) \\ +k_3 s_1 + \varepsilon|x_1|^{\lambda_2} s_1 \end{pmatrix} |s_1| \leq 1 \end{cases} \quad (41)$$

In summary, we obtain the model-free Enhanced sliding mode controller (ESMC) for the YASA-AFFSSPM motor system as shown in Figure 2. The feedback controller u_c in the controller incorporates the improved sliding mode control law with the enhanced double power combination reaching law. The disturbance F is observed in real-time by the extended sliding mode disturbance observer.

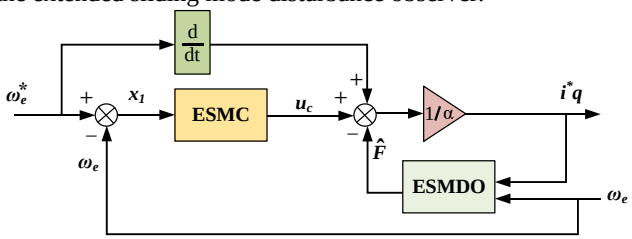

Fig. 2 Enhanced model-free sliding mode controller.

IV. Simulation Results and Analysis

In order to further verify the feasibility of the IMFSMC algorithm and its better robustness against load disturbances and parameter perturbations, a MATLAB/SIMULINK model was constructed to compare and verify the simulation results of the EMFSMC, MFSMC, control algorithms. parameters of 12S/19P YASA-AFFSSPM motor are shown in table 1. After conducting a theoretical analysis of the vector control technology for permanent magnet synchronous motors, in this paper simulation models are constructed to the SVPWM module, coordinate transformation module, and proposed control module within the vector control system. Ultimately, these modules are integrated to complete the simulation of a dual closed-loop vector control system with id = 0. The analysis also examines the responsiveness and stability of the system based on the mathematical model of the motor in the dq axes. The system control block diagram of traditional MFSMC and EMFSMC motor are shown in the Fig. 3. Moreover, motor parameter settings are shown in the Table1. The parameters of the control methods are as follows. EMFSMC parameters: k_1=10, k_2=200, k_3=10, ε_1= 0.1, ε_2=0.55, α=1, c=70, λ_1=1.5, λ_2=0.5, β=1.5, ζ=10, l=1, δ=100. MFSMC parameters: k_1=10, k_2=200, k_3=10, ε_1= 0.1, ε_2=0.55, α=1, c=70, λ_1=1.5, λ_2=0.5, β=1.5.

A. *Analysis of simulation results under parameter perturbation*

Setting the initial torque of the motor to 0 N.m, at 0.2 s, the torque increases to 10 N.m. Setting the initial value of the rotor flux to 0.062 Wb, at 0.1 s, the rotor flux decreases to 0.042 Wb. The q-axis inductance of the motor decreases from 0.47 mH to 0.29 mH at 0.3 s. Figure 4 shows the motor speed response curve. It shows the simulation results of the 12S/19P YASA-AFFSSPM control system under the Traditional MFSMC and EMFSMC controllers.

TABLE. 1: 12S/19P YASA-AFFSSPM MOTOR PARAMETERS

Parameter	Symbol	Value	Unit
d-axis inductance	L_d	0.2e-3	H
q-axis inductance	L_q	0.47e-3	H
DC bus voltage	U_{dc}	311	V
Rotor flux	Ψ	0.062	Wb
Phase resistance	R	0.025	Ω
Load torque	T	12	N·m
Moment of inertia	J	0.00302	Kg.m^2

With the MFSMC controller, it takes a long time for the motor to reach the preset speed from a no-load start, approximately 0.04 seconds, with a significant overshoot of about 12.5%. Compared with traditional MFSMC control, with the EMFSMC controller 12S/19P YASA-AFFSSPM response time is significantly reduced, about 0.015s, and it reaches the given speed quickly without overshoot.

At 0.1 s when the rotor flux decreases, the speed curve of EMFSMC is also superior to MFSMC, with the speed curve of EMFSMC stabilizing after 0.08 s following a 0.1 rpm fluctuation, while MFSMC control requires 0.05 s to stabilize after fluctuations of 0.15 rpm, showing inferior performance compared to EMFSMC. At 0.3 s, when the q-axis suddenly decrease, the speed curve of EMFSMC shows even smaller speed fluctuations compared to MFSMC control method. Therefore, it is evident that in speed control, EMFSMC is more precise and stable than MFSMC. When a load of 10N·m is suddenly added to the 12S/19P YASA-AFFSSPM at 0.2s, the MFSMC control produces a rotational speed drop of about 9 rpm, and returns to the steady state after about 0.03s; the rotational speed drop using the improved EMFSMC control is only about is 4 rpm, and the speed recovery time is shortened to about 0.01s. Figure 5 shows the torque response curves of the two control methods.

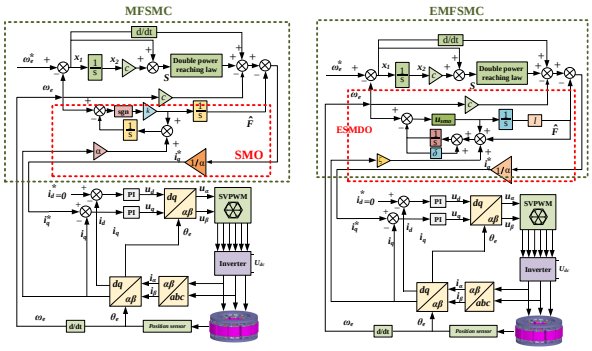

(a) (b)

Fig. 3 Control block diagram. (a) Traditional MFSMC (b) EMFSMC.

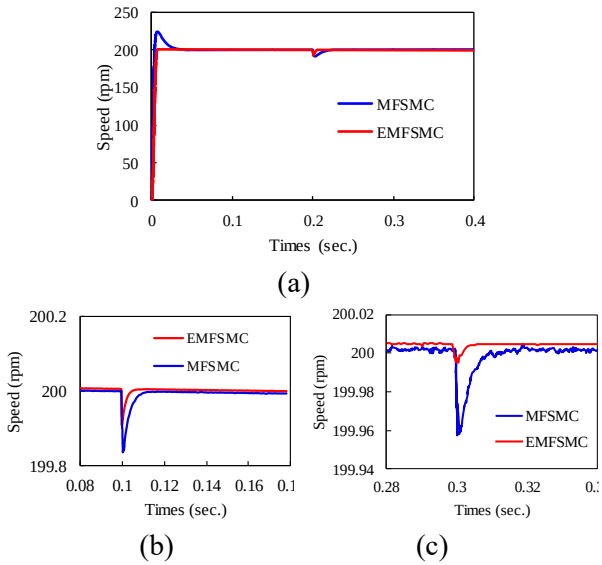

(a)

(b) (c)

Fig4. Comparison of the speed (a) Global speed comparison waveforms (b) Local magnified waveforms under demagnetization fault at t=0.1sec. (c) Local magnified waveforms under decrease of q-axis inductance. at t=0.3sec.

From the analysis of Figure 6 (a), it can be seen that the three-phase current waveform when using the MFSMC controller has obvious current distortion, while the current waveform of Figure 6 (b) when using the EMFSMC controller is smoother and close to sinusoidal wave.

Through comparison, it can be seen that the torque ripple under the MFSMC controller is larger, about 1.6N·m, while using the EMFSMC controller, the torque ripple is significantly reduced, about 1N·m and the dynamic response speed of the motor's electromagnetic torque is significantly improved. Figure 6 shows the current response waveform before and after the load torque changes suddenly.

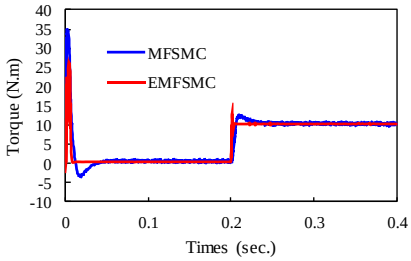

Fig. 5 Torque response curve

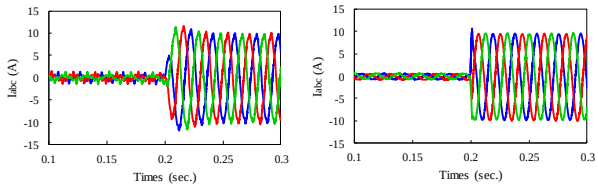

(a) (b)

Fig. 6 Three-phase current response curve (a) MFSMC controller (b) EMFSMC controller

Figure 7 is a comparative simulation diagram when the speed control system starts without load and the speed suddenly changes to 400r/min in 0.2s. Through analysis, it can be seen that the EMFSMC controller proposed in this article can be used under variable speed conditions, and the speed regulation performance is relatively ideal. Compared with the MFSMC controller, it can significantly reduce the overshoot phenomenon after a large speed mutation, and quickly reach the given rotating speed value.

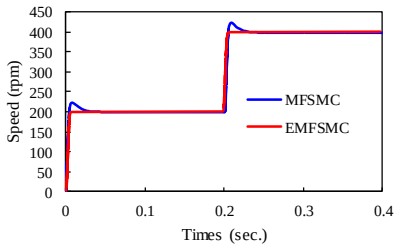

Fig. 7 Speed response curve.

V. Experimental Results

In order to evaluate the performance of the proposed control on 12S/19P YASA-AFFSSPM motor, a prototype motor is manufactured. The system employs vector control, facilitated by a three-phase converter, with the vector control algorithm implemented through a MicroLab digital controller. Figure 8 depicts the experimental arrangement for the proposed method.

In the experiment, the initial torque of the motor is set to 5 *Nm*, and at 0.2 seconds, the torque increases to 15 Nm. The initial value of the motor rotor magnetic flux linkage is set to 0.062 Wb, which decreases to 0.042 Wb at 0.3 seconds.

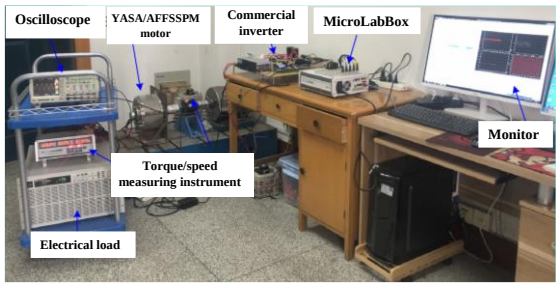

Fig. 8. Motor testing platform.

The q-axis inductance of the motor decreases from 0.47 mH to 0.29 *mH* at 0.4 seconds, while the d-axis inductance decreases from 0.2 *mH* to 0.14 *mH* at 0.5 seconds. The motor resistance increases to 0.035 Ω at 0.6 seconds. Figures 9, 10, and 11 illustrate the experimental waveforms of the d-q axis currents, speed, and torque for the MFSMC and EMFSMC control methods under motor parameter perturbations. To ensure consistency, the parameter design and parameter perturbation time were aligned with the parameters used in the simulation experiments.

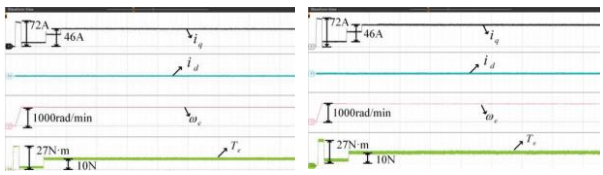

200 m/s 200 m/s

(a) (b)

Fig. 9. waveforms under load and parameter disturbances. (a) EMFSMC. (b) MFSMC.

Upon analyzing the experimental results, it can be seen that the overall trend and effectiveness of the semi-physical experiment are consistent with the simulation. In comparison of Figures 10(a) and 10(b), after 0.05 seconds of motor startup, when the speed stabilizes at 1000 rad/min, the speed fluctuation of EMFSMC is only ±0.004 rad/min, whereas the speed fluctuation for the MFSMC control method is ±0.03 rad/min. Therefore, the speed curve of the EMFSMC is smoother and exhibits less jitter compared to that of the MFSMC control method. Similarly, when the torque stabilizes at 15 N·m, the torque variation of EMFSMC is ±1.5 N·m, while the torque fluctuation for MFSMC control is greater, at ±2.5 N·m. Thus, it is evident that the torque experimental waveform variation of the EMFSMC is smaller than that of the MFSMC control, showcasing stronger

robustness. Comparing Figures 11(a) and 11(b), which depict the d-q axis current experimental waveforms for EMFSMC and MFSMC control, we observe that after approximately 0.45 seconds of parameter perturbation and once the current reaches stability, the variation in the q-axis current for EMFSMC is ±2.5 A, while the variation for the MFSMC control method is ±3.1 A.

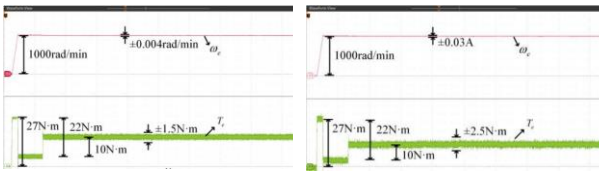

200 m/s (a) 200 m/s (b)

Fig. 10. Speed and torque waveforms. (a) EMFSMC. (b) MFSMC.

Therefore, the magnitude of the current experimental waveform variation for EMFSMC is smaller than that of the MFSMC control. Thus, whether comparing the speed and torque experimental waveforms or the current experimental waveforms, IMFSMC exhibits smaller fluctuations and operates more stably under both steady-state conditions and parameter perturbations.

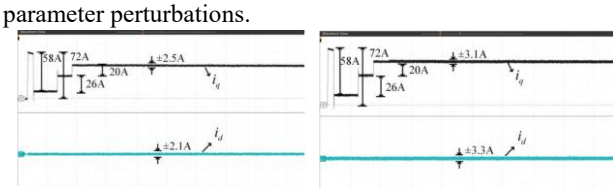

200 m/s (a) 200 m/s (b)

Fig. 11. d-q axis current waveforms. (a) EMFSMC. (b) MFSMC.

Quantitative and qualitative comparison between EMFSMC and MFSMC is given in Table 2. In summary, the EMFSMC method, while more complex and requiring more parameters, offers superior convergence speed and robustness against disturbances compared to both MFSMC and traditional PI control. The MFSMC provides a balance between complexity and performance but falls short in speed and robustness. PI control remains the simplest but is less effective in dynamic applications where precision and responsiveness are critical.

TABLE 2: COMPARISON BETWEEN EMFSMC AND MFSMC.

Criterion	EMFSMC	MFSMC
Time response	~0.015S	~0.04 sec.
Overshoot	At least	~12.5%
Speed drop under sudden load	~4 rpm	~9 rpm
Recovery time to steady state	~0.01 sec.	~0.03 sec.
Speed fluctuations	~0.1 rpm	~0.15 rpm
Torque fluctuations	~1 N·m	~1.6 N·m
Current fluctuations	±2.5 A	±3.1 A
Response to load changes	Fast and stable	Slow and unstable
Control accuracy	higher	lower
Strength against disturbances	higher	lower

VI. Conclusion

Considering the impact of external conditions on motor parameter perturbations that reduce the robustness of speed loop control systems, an Enhanced Model-Free Sliding Mode Control (EMFSMC) algorithm is proposed. The following conclusions are drawn from mathematical analysis and experimental verification: 1) An improved double-power combination sliding mode reaching law is employed to redesign the sliding mode controller, enhancing system stability and reducing chattering typical of traditional reaching laws. 2) Integrating the Extended Sliding Mode Disturbance Observer (ESMDO) with the improved model-free sliding mode controller enables real-time estimation of unknown disturbances in the speed loop, significantly boosting the motor system's response capability. Specifically, EMFSMC reduces speed response time from approximately 0.04 seconds with Model-Free Sliding Mode Control (MFSMC) to about 0.015 seconds, marking an improvement of approximately 62.5%. Under sudden load conditions, speed drop is minimized from 9 rpm with MFSMC to 4 rpm with EMFSMC, achieving a reduction of about 55.6%. The recovery time to stability is also enhanced, decreasing from 0.03 seconds with MFSMC to 0.01 seconds with EMFSMC, a 66.7% improvement. These enhancements in speed response, stability, and robustness highlight the effectiveness of EMFSMC in dynamic applications, especially in electric vehicles and precision-demanding industries.

REFERENCES

[1] J. F. Gieras and J.-X. Shen, *Modern Permanent Magnet Electric Machines*. CRC Press, 2022.

[2] FNU Nishanth, Joachim Van Verdeghem, and E. L. Severson, "A Review of Axial Flux Permanent Magnet Machine Technology," *IEEE Transactions on Industry Applications*, vol. 59, no. 4, pp. 3920–3933, Jan. 2023.

[3] J. R. Fard and M. Ardebili, "Design and Control of a Novel Yokeless Axial Flux-Switching Permanent-Magnet Motor," *IEEE Transactions on Energy Conversion*, vol. 34, no. 2, pp. 631–642, Jun. 2019.

[4] J. Rahmani Fard and M. Ardebili, "Optimal Design and Analysis of the Novel Low Cogging Torque Axial Flux-Switching Permanent-Magnet Motor," *Electric Power Components and Systems*, vol. 46, no. 11–12, pp. 1330–1339, Jul. 2018.

[5] A. Brosch, O. Wallscheid, and Joachim Böcker, "Time-Optimal Model Predictive Control of Permanent Magnet Synchronous Motors Considering Current and Torque Constraints," *IEEE Transactions on Power Electronics*, vol. 38, no. 7, pp. 7945–7957, Apr. 2023.

[6] S. Lin, Y. Cao, C. Li, Z. Wang, T. Shi, and C. Xia, "Two-Degree-of-Freedom Active Disturbance Rejection Current Control for Permanent Magnet Synchronous Motors," *IEEE Transactions on Power Electronics*, vol. 38, no. 3, pp. 3640–3652, Nov. 2022.

[7] X. Sun, F. Cai, Z. Yang, and X. Tian, "Finite Position Control of Interior Permanent Magnet Synchronous Motors at Low

Speed," *IEEE Transactions on Power Electronics*, vol. 37, no. 7, pp. 7729–7738, Jul. 2022.
[8] J. Yim, S. You, Y. Lee, and W. Kim, "Chattering Attenuation Disturbance Observer for Sliding Mode Control: Application to Permanent Magnet Synchronous Motors," *IEEE transactions on industrial electronics*, vol. 70, no. 5, pp. 5161–5170, May 2023.
[9] J. Huang, X. Zhu, Y. Li, G. Qi, Y. Wu, and Y. He, "A New Composite Sensorless Control Strategy for PMSM Used in Electric Vehicle," *2022 IEEE Transportation Electrification Conference and Expo, Asia-Pacific (ITEC Asia-Pacific)*, Oct. 2022.
[10] M. R. Shokoohinia and M. M. Fateh, "Model-Free Tracking Control via Adaptive Dynamic Sliding Mode Control With Application To Robotic Systems," *International Journal of Industrial Electronics Control and Optimization*, vol. 3, no. 4, pp. 431–438, Sep. 2020.
[11] C. Gao, J. Dai, J. Li, and J. Li, "Finite-Time Convergence ESO-Based Nonsingular Fast Terminal Sliding Mode Control for PMSM with Unknown Parameters and Time-Varying Load," *Mathematical Problems in Engineering*, vol. 2022, pp. 1–13, Nov. 2022.
[12] D. Jin, L. Liu, S. Liu, and D. Liang, "Modified Deadbeat Predictive Current Control for PMSM Drive System via a Composite Integral Sliding Mode Observer," *2022 IEEE Energy Conversion Congress and Exposition (ECCE)*, pp. 1–8, Oct. 2022.
[13] Y. Wei, D. Ke, X. Yu, F. Wang, and José Rodríguez, "Adaptive Inertia Observer-based Model-Free Predictive Current Control for PMSM Driving System of Electric Vehicles," *IEEE Transactions on Industry Applications*, vol. 60, no. 4, pp. 6252–6262, May 2024.
[14] A. Rezaie, "Sliding Mode Control for Chaotic Systems with Unknown Uncertainties," *International Journal of Industrial Electronics Control and Optimization* , vol. 7, no. 1, pp. 53–60, Mar. 2024.
[15] Z. Zhang, Q. Xu, and Y. Wang, "A New Sliding-Mode Observer-Based Deadbeat Predictive Current Control Method for Permanent Magnet Motor Drive," *Machines*, vol. 12, no. 5, pp. 297–297, Apr. 2024.
[16] J. Yim, S. You, Y. Lee, and W. Kim, "Chattering Attenuation Disturbance Observer for Sliding Mode Control: Application to Permanent Magnet Synchronous Motors," *IEEE transactions on industrial electronics*, vol. 70, no. 5, pp. 5161–5170, May 2023.
[17] X. Wang, Q. Xu, Y. Whang, X. Zhang, S. Liu, and Y. Miao, "Model-Free Predictive Current Control of PMSM Based on Sliding Mode Disturbance Observer," *2021 24th International Conference on Electrical Machines and Systems (ICEMS)*, pp. 3739–3744, Nov. 2023.
[18] A. Razzaghian , R. Kardehi , and N. Pariz, "Adaptive fuzzy fractional-order fast terminal sliding mode control for a class of uncertain nonlinear systems," *International Journal of Industrial Electronics Control and Optimization* , vol. 5, no. 1, pp. 77–87, Mar. 2022.
[19] X. Sun, J. Cao, G. Lei, Y. Guo, and J. Zhu, "A Composite Sliding Mode Control for SPMSM Drives Based on a New Hybrid Reaching Law With Disturbance Compensation," *IEEE Transactions on Transportation Electrification*, vol. 7, no. 3, pp. 1427–1436, Sep. 2021.
[20] W. Li, H. Yuan, S. Li, and J. Zhu, "A Revisit to Model-Free Control," *IEEE transactions on power electronics*, vol. 37, no. 12, pp. 14408–14421, Dec. 2022.

Javad Rahmani-Fard received the B.S. degree from Shahed University, Tehran, Iran, in 2009, and the M.S. and Ph.D. degrees in electrical engineering from the K.N. Toosi University of Technology, Tehran, in 2012 and 2018, respectively. Currently, he is an assistant professor of the electrical engineering at Qom University of Technology, Qom, Iran. His research interests include the analysis and design of electrical machines, and sensor-less variable-speed drives, multiphase variable-speed drives.

Saeed Hasanzadeh received the B.S. degree from Shahroud University of Technology, Shahroud, Iran, in 2003, and the M.Sc. and Ph.D. degrees from University of Tehran, Tehran, Iran, in 2006 and 2012, respectively, all in electrical engineering. He joined the faculty of Electrical and Computer Engineering, Qom university of Technology as an Assistant Professor in 2013. His research interests include Power Electronics, Inductive Power Transfer Systems, Electrical Machines and Drives, Electric Vehicles, Magnetic Levitation Systems.